Polymer 52 (2011) 1133–1140

Contents lists available at ScienceDirect

Polymer

journal homepage: www.elsevier.com/locate/polymer

Crystal growth pattern changes in low molecular weight poly(ethylene oxide) ultrathin films

Guoliang Zhang [a], Yan Cao [b], Liuxin Jin [a], Ping Zheng [a], Ryan M. Van Horn [b], Bernard Lotz [c,**], Stephen Z.D. Cheng [b,*], Wei Wang [a,**]

[a] The Key Laboratory of Functional Polymer Materials of Ministry of Education and Institute of Polymer Chemistry, College of Chemistry, Nankai University, Tianjin 300071, China
[b] Department of Polymer Science, College of Polymer Science and Polymer Engineering, The University of Akron, Akron, OH 44325-3909, USA
[c] Institut Charles Sadron, 23 Rue du Loess, BP 84047, Strasbourg 67034, France

ARTICLE INFO

Article history:
Received 18 November 2010
Accepted 3 January 2011
Available online 9 January 2011

Keywords:
Ultrathin film
PEO
Crystal pattern

ABSTRACT

A low molecular weight (MW) poly(ethylene oxide) (PEO) crystallized in ultrathin films displays various crystal growth patterns in a crystallization temperature (T_x) range from 20.0 °C to 50.0 °C. In succession, the following patterns are found: nearly one-dimensional (1D) dendrite-like crystal patterns at $T_x \leq 38.0$ °C, two-dimensional (2D) seaweed-like patterns between 39.0 °C $\leq T_x \leq$ 42.0 °C and again, nearly 1D dendrite-like patterns at $T_x \geq 43.0$ °C. These transitions result from a complex interplay of varying growth rates along different growth directions and preservation of growth planes. Structural analysis carried out via electron diffraction indicates that the dendrite-like crystals formed at the low and high T_x values differ by their fast growth directions: along the {120} normal at the low T_x values and along the (100) and (010) normal at the high T_x values. In the later case however, the major growth faces are still the {120}, this time tilted at 45° and indicating the a^* and b axes growth tips. In the intermediate T_x range (39.0 °C–42.0 °C), three growth directions coexist giving rise to the seaweed morphology. The crystal growth rates at the low and high T_x values are constant versus time. For the seaweed, a square-root dependence is obtained. These differences are probably due to 1D and 2D growth in the ultrathin films and are associated with different growth patterns of the dendrites and the seaweed, respectively.

1. Introduction

Crystallization of polymers is one of the most intriguing topics in macromolecular physics [1,2]. Due to their long-chain nature, polymer chains kinetically prefer to fold back and forth to form metastable folded-chain lamellar crystals under supercooled conditions [1–4]. The shape of single crystals may change with crystallization conditions (solution, bulk, crystallization temperature (T_x), and others) due to the different dependencies of the growth rates of different crystallographic planes. For example, single crystals of polyethylene (PE) show a lozenge or truncated lozenge shape in good solvent and even a lenticular habit in poor solvent at high T_x [2,5–8]. Toda observed that PE single crystals grown in the bulk change from truncated lozenge to lenticular shape with increasing T_x [9,10]. Kovacs et al. and Cheng et al. found that the shape of poly(ethylene oxide) (PEO) single crystals change from a faceted habit to rounded and back to faceted in a T_x range near the equilibrium melting temperature [11–14].

Recently, polymer crystallization in thin and ultrathin films has attracted increasing attention for both practical and scientific reasons [15–36]. Crystallization in ultrathin films is very different from bulk crystallization. Monolayer 2D lamellar crystals are formed in ultrathin films as opposed to three-dimensional (3D) spherulites in the bulk. Furthermore, different types of crystal shapes (*e.g.* labyrinthine, dendrite, seaweed, compact and faceted single crystals) have been observed in polymer ultrathin films [16–18,22,23,25,31,32,34,35]. A transition from dendrite to seaweed in PEO ultrathin films has also been observed [16,25,28], although the crystallographic relationship and the underlying reason of the transition are still obscure [36–51]. It is accepted that the differences in growth anisotropy are the origin of the different pattern formations [38,41]. A gradual change in the growth anisotropy may result in a progressive pattern evolution from dendrite to seaweed or from one to another dendrite [25,37,39–45,49,52]. Although theoretical studies have illustrated the pattern selection principle in some aspects of growth kinetics [44,45], the limited set

* Corresponding author. Tel.: +1 330 972 7539; fax: +1 330 972 6581.
** Corresponding authors.
E-mail addresses: guoliang2008@mail.nankai.edu.cn (G. Zhang), yc41@uakron.edu (Y. Cao), jlx115@mail.nankai.edu.cn (L. Jin), zhengping@nankai.edu.cn (P. Zheng), rmv4@uakron.edu (R.M. Van Horn), bernard.lotz@ics-cnrs.unistra.fr (B. Lotz), scheng@uakron.edu (S.Z.D. Cheng), weiwang@nankai.edu.cn (W. Wang).

0032-3861/$ – see front matter © 2011 Elsevier Ltd. All rights reserved.
doi:10.1016/j.polymer.2011.01.002

of experimental data is still insufficient to obtain a universal morphological diagram based on an in-depth understanding of the origin of pattern selections [17,25,31,32,37,39–42,49,52].

In this work, we describe and analyze a dendrite-seaweed-dendrite crystal evolution in ultrathin films of a low molecular weight (MW) PEO in the 20.0–50.0 °C T_x range. Atomic force microscopy (AFM) was used to observe crystal morphologies. Transmission electron microscopy (TEM), and more specifically electron diffraction (ED) patterns helped to determine the crystal growth directions and growth planes. Crystal growth rates were measured at different T_x in order to analyze the formation mechanisms of the dendrite and seaweed crystals. The possible origin of crystal growth pattern evolution is discussed.

2. Experimental section

A PEO fraction with weight-average molecular weight ($\overline{M}_w$) 7.2×10^3 g/mol and polydispersity index (PDI) 1.01 was purchased from Polymer Source. The two end groups are a methyl group and a hydroxyl group. Its equilibrium melting temperature is $T_m^0 = 64.1$ °C [53]. A toluene solution of PEO ($c = 0.01\%$ w/v) was prepared for film deposition.

Square 0.8 × 0.8 cm^2 silicon wafers were treated in Piranha solution of H_2SO_4 (98%): $H_2O_2 = 3{:}1$ at 120 °C for 30 min to provide a layer of –OH groups on the silicon surface. These substrates were then cleaned in an ultrasonic water bath. The contact angle, θ, of water on treated silicon wafer was $\theta = 8°$. Silicon monoxide substrates supported by copper grids were purchased from Ted Pella Inc for TEM experiments.

Ultrathin PEO films were prepared by drop-casting the solution onto the silicon wafer or the copper grid supported silicon monoxide. The samples were dried at ambient condition and then treated in vacuum for 12 h. The as-prepared samples were heated to 80.0 °C for 10 min to form a uniform molten layer of 3–4.5 nm thick (measured by AFM). They were then cooled to a preset T_x for isothermal crystallization for 12 h. The samples were then cooled to room temperature for AFM and TEM examination.

Crystal growth patterns were imaged with a hot-stage multimode AFM (Digital Instrumental Nanoscope IV). The tapping mode was used to obtain height and amplitude images. The cantilever force was adjusted to a set-point value of 1.3–1.5 V to limit damage to the sample. The scanning rate was 1.0–1.2 Hz for low-magnification images at a resolution of 512 × 512 pixels/image. Taking advantage of in-situ and real-time observations on polymer crystallization using AFM [54–58], kinetic growth experiments were performed in a T_x range of 34.0 °C ≤ T_x ≤ 50.0 °C. When T_x < 34.0 °C, the growth is difficult to track because the AFM tip induces many nuclei around the growing tips. For fast crystal growth kinetics, resolutions of 128 × 128 pixels or 256 × 256 pixels/image and a scanning rate of 1.5 Hz were used.

Crystals were also observed using TEM (Philips Tecnai) at an accelerating voltage of 120 kV. Selected area electron diffraction (SAED) experiments were carried out to determine crystal growth directions and growth planes. The *d*-spacings were calibrated using a TlCl standard. Molecular modeling and analysis of the diffraction patterns were performed using the Cerius^2 package of Accelrys.

3. Results and discussion

3.1. Evolution of crystal patterns with crystallization temperatures

Fig. 1a–f shows six AFM amplitude images of the PEO crystals at T_x's ranging from 20.0 °C to 49.0 °C. Ribbon-like branches are indicative of the preferred growth directions. Fig. 1a represents a typical dendrite-like crystal formed at $T_x = 20.0$ °C with primary, secondary, and sometimes even tertiary branches. These branches possess narrow backbones along the center line (denoted as B-branches). The angles between the primary and secondary branches or between secondary and tertiary branches are all 90°. The crystals formed at $T_x = 37.0$ °C (Fig. 1b) are almost identical to those in Fig. 1a. Yet, some of the branches do not display their recognized backbones along the central line (denoted as NB-branches). The angles between the B- and NB-branches are at 45°. On average, the 90° angle between primary and secondary B-branches is dominant. When crystallization takes place at $T_x = 40.0$ °C (Fig. 1c), numerous B- and NB-branches grow alternately and thus, lead to a seaweed-like crystal. Again, the angles between the B- and NB-branches are 45°. At $T_x = 44.0$ °C (Fig. 1d), the NB-primary branches become the major population with NB-secondary branches. The branching angles between NB-branches are always 90°. B-branches at a 45° angle to the NB-secondary branches exist only in tertiary branches. When increasing T_x to 46.0 °C (Fig. 1e), a new type of dendrite-like crystal appears. It is only composed of NB-branches with a 90° branching angle. At $T_x = 49.0$ °C (Fig. 1f), crystals have a typical dendrite-like shape with four branches and approximately a four-fold symmetric structure.

These AFM images illustrate a transition from one type of dendrite crystal to another dendrite type with a seaweed crystal as an intermediate stage with increasing T_x. The angles between branches of the same kinds (either within the B- or NB-type) are 90°, while those between B- and NB-branches are 45°. Furthermore as shown in Fig. 2, the backbone width in the B-braches is T_x dependent. At $T_x = 20.0$ °C, the width is ~50 nm, and it increases to ~320 nm at 45.0 °C. Fig. 3 shows the thickness H_c of the backbone and the periphery in the B-branches and, the thickness of NB-branches. Backbone thickness increases from 7.2 nm at $T_x = 20.0$ °C to 9 nm at $T_x = 30.0$ °C. The 9 nm value corresponds to a quadruple-folded-chain crystal. The thickness then suddenly increases to 11 nm at $T_x = 36.0$ °C and further to 15 nm at 43.0 °C, which suggests that the chains fold three and two times, respectively [59]. It should be noted however that the thickness of the backbone in B-branches is generally 1 nm thicker than the periphery until $T_x = 45.0$ °C. Specifically, these two thickness values are in the non-integral folding stage at lower T_x and increase in a quantized fashion based on integral folding at higher T_x. Beyond 46.0 °C, the B-branches disappear, and the dendrites are only composed of NB-branches. The NB-branch thickness reaches 15 nm (twice-folded integral chains). Further increase to $T_x = 50.0$ °C leads to a substantial increase of the thickness, indicating that the number of folds decreases, although the H_c value does not yet reach the expected extended chain length.

Upon analysis of the crystal growth patterns of dendrites and seaweeds and the determination of backbone and lamellae thickness, it appears that we are dealing with a complex growth pattern. The crystal growth kinetics in ultrathin films depend on diffusion of crystallizable molecules as well as on the tendency of PEO chains to crystallize in integrally quantized stem lengths that are two, three and four times smaller than the chain length. Only for fast growth rates, especially for $T_x < 30.0$ °C, are the PEO chains in the crystal non-integrally folded [59,60].

3.2. Crystal growth directions

The PEO crystal structure and chain conformation are well known (Fig. 4a): four distorted 7_2 helical molecules are packed in a monoclinic unit cell, $a = 0.805$ nm, $b = 1.304$ nm, $c = 1.948$ nm and $\beta = 125.4°$ [61]. It turns out that $a \times \sin\beta = 0.656$ nm is only nearly half of the *b* dimension in the *c* axis projection. In most (but not all) growth processes, therefore, the PEO crystal lies on an apparent tetragonal projection. Prominent crystallographic planes are thus 90° apart, *e.g.* (120) and $(1\bar{2}0)$, or (100) and (010). This explains the nearly square

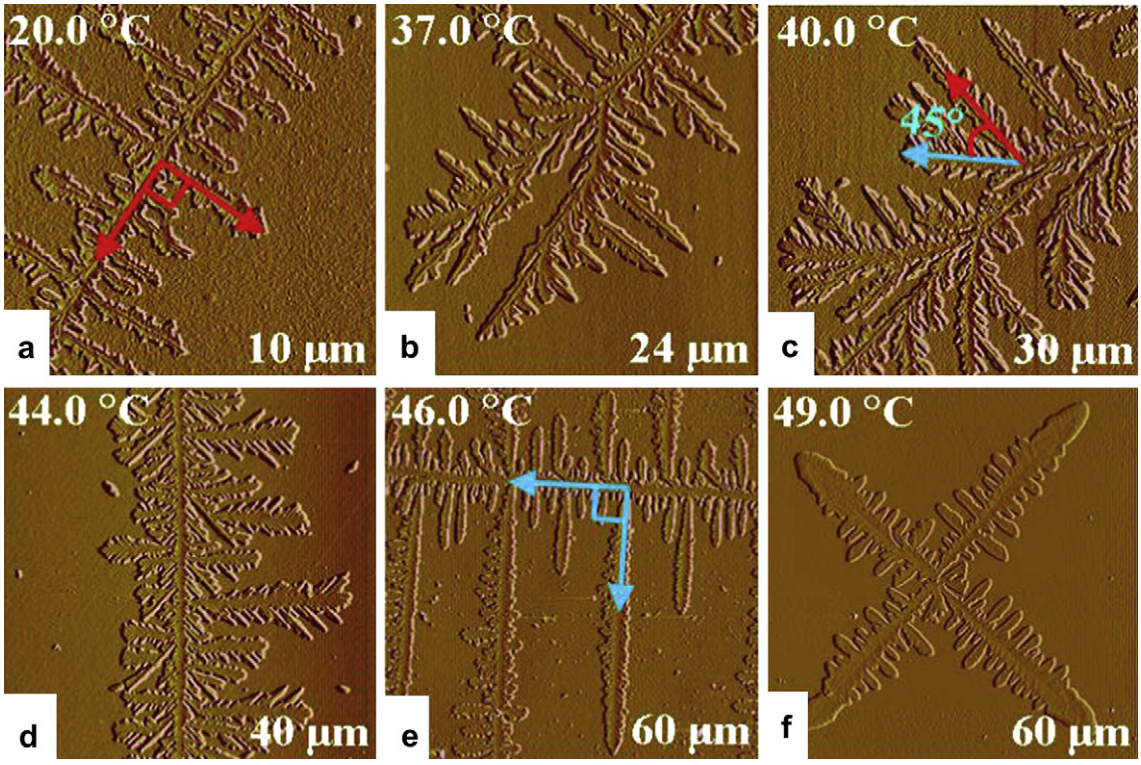

Fig. 1. A set of AFM amplitude images showing crystal growth pattern evolution as a function of T_x. Red and blue arrows represent B-branches and NB-branches respectively, and the angles between them are 90° or 45°. (For interpretation of the references to colour in this figure legend, the reader is referred to the web version of this article).

shape of solution grown crystals, and the existence of branches at 90° in dendrite growth. Because of this apparent high symmetry, it is not possible to determine the crystallographic axes in the dendrite on morphological outline alone. Such a determination requires, in this case, SAED. Fig. 4b shows the calculated (hk0) diffraction pattern of PEO from the Cerius[2] model. The four strongest diffractions correspond to densely packed (120) planes. The six weaker spots close to the center help to determine a^* and b axes. We expect that the observed angle selections between branches should be related to the growth directions along the <120>, the a^* and b axes [28,62,63].

The SAED patterns in correct orientation to the dendrite and seaweed crystals are shown in Fig. 5a. Analysis of the figures reveals the essential difference between the dendrites grown at the low and the high T_x values, in spite of their similar morphologies. In the low T_x dendrites, the branches are parallel to the <120>, whereas for high T_x, the branches are extended along the a^* and b axes (compare the dendrites at $T_x = 26.0$ °C and 46.0 °C). In other words, the major growth directions are 45° away for the low and high T_x dendrites. Dendrites composed of B-branches are denoted $DB_{(120)}$, while dendrites composed of NB-branches are denoted $DNB_{(100)/(010)}$. At intermediate T_x, between 38.0 °C and 43.0 °C, three growth directions coexist. They give rise to more ill defined morphologies, with curved growth faces, characteristic of the seaweed patterns, although they yield clear single crystal ED patterns. Note however that a^* and b axes can be differentiated only via SAED experiments.

To summarize the morphological transition of the PEO crystals, three T_x regions are obtained as follows (Fig. 5b): At $T_x \leq 38.0$ °C, $DB_{(120)}$ dendrites with a backbone in preferential growth directions

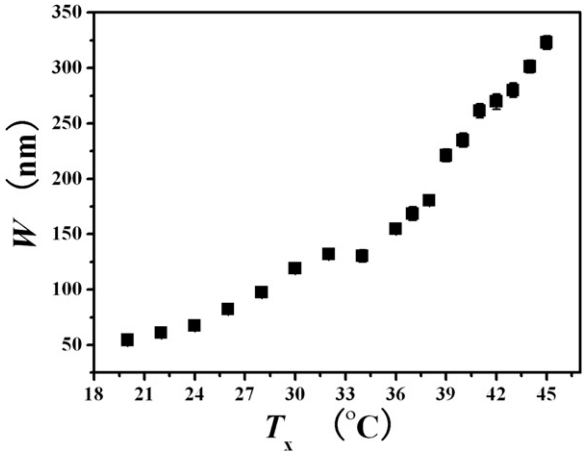

Fig. 2. Width (W) of the backbone in B-branches as a function of T_x.

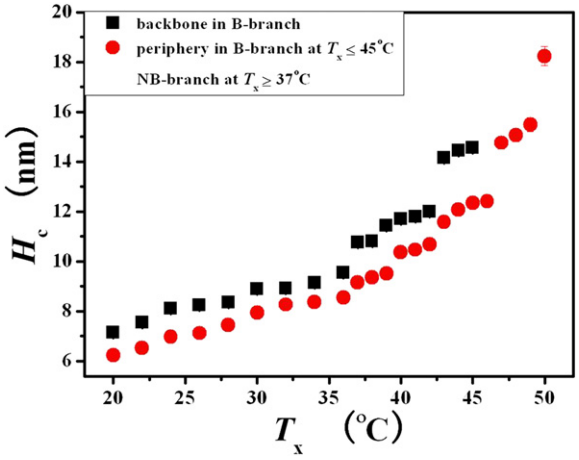

Fig. 3. Thickness (H_c) of crystal as a function of T_x. ■ represents the thickness of backbone in B-branch. ● represents the thickness of the periphery in the B-branch at $T_x \leq 45.0$ °C and the thickness of the NB-branch at $T_x \geq 37.0$ °C. In the region 37.0 °C $\leq T_x \leq$ 45.0 °C, the thickness of the periphery in the B-branch is equal to the thickness of the NB-branch.

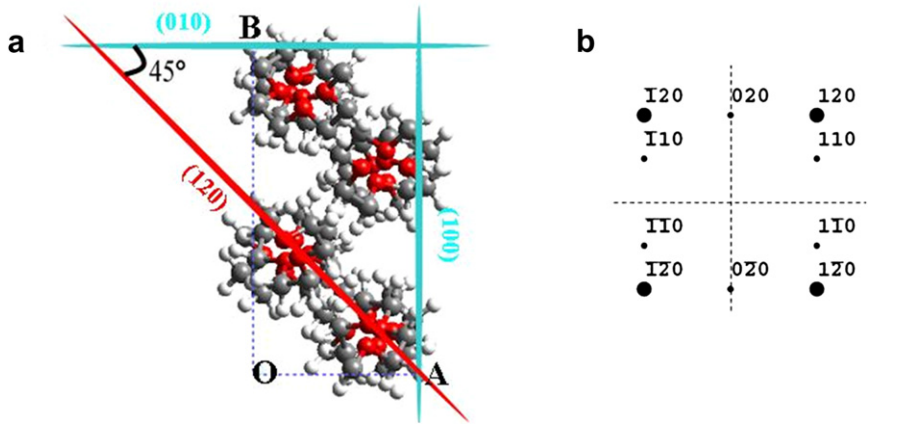

Fig. 4. (a) Unit cell of PEO crystal in the direction of *c* axis. The angle between the {120} and the (100) or (010) planes is 45°. (b) Calculated [001] zone ED pattern.

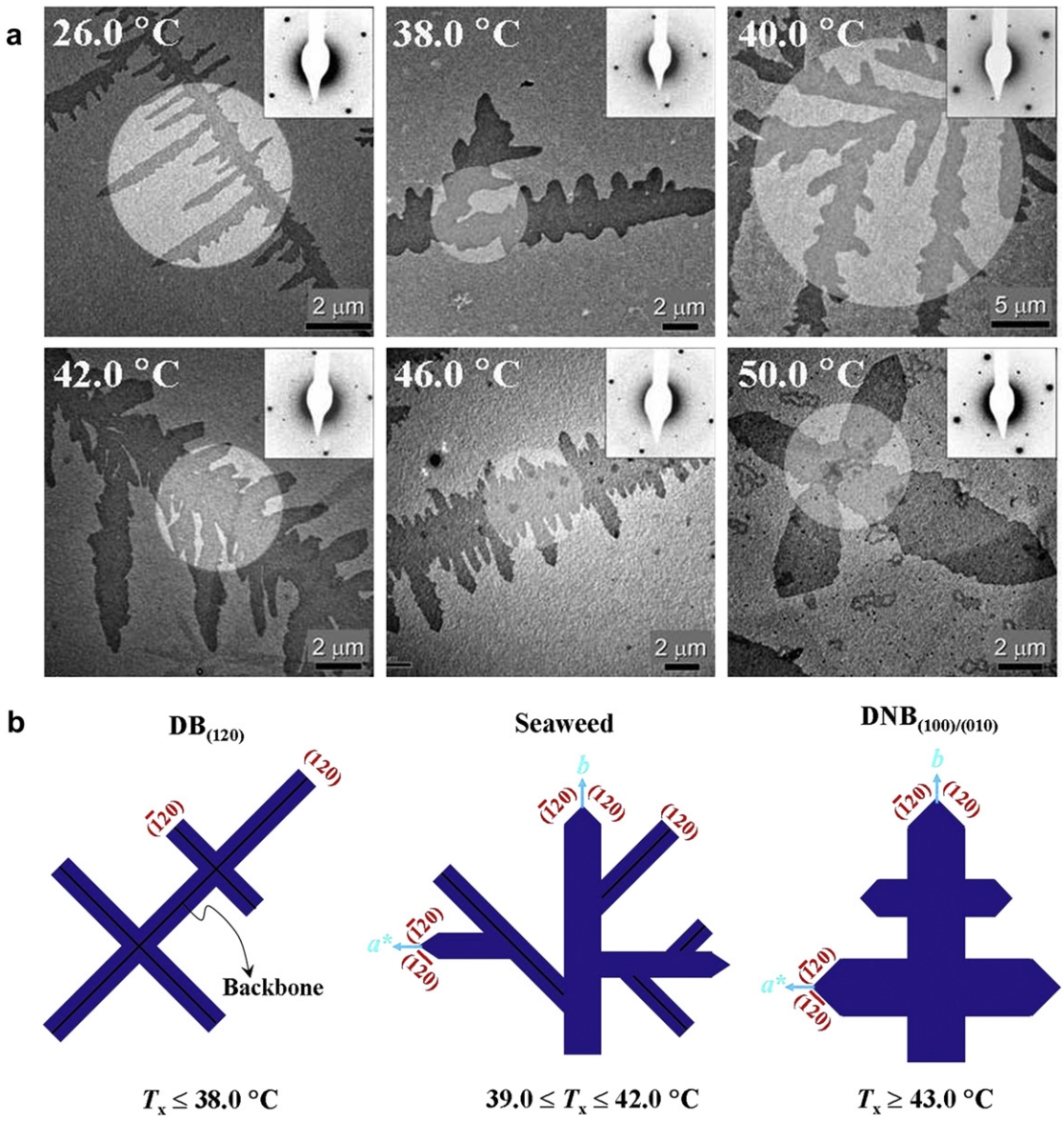

Fig. 5. (a) TEM images and SAED patterns at different T_x. (b) Schematics showing crystal growth direction changing from the <120> to a^* and b axes with increasing T_x.

along the <120> and a 90° branching angle; at 39.0 °C ≤ T_x ≤ 42.0 °C, seaweed with growth direction along the <120> and the a^* and b axes and a 45° branching angle; at T_x ≥ 43.0 °C, $DB_{(100)/(010)}$ dendrites with preferential growth direction along the a^* and b axes and a 90° branching angle.

3.3. Crystal growth rate and mechanisms

In-situ experiments were performed using AFM to determine the crystal growth rates. AFM is useful in the high T_x range since homogeneous nucleation is difficult in this T_x region, while the AFM tip can induce the crystal nucleation. The results indicate a significant difference between the growth rate time dependencies of both the low and high T_x dendrites on one side and seaweed on the other.

For the dendrites in both temperature regions of $T_x \leq 38.0$ °C and $T_x \geq 43.0$ °C, the length of the primary branches, R, along the <120> and the a^* and b axes are linearly proportional to time (t) as shown in Figs. 6 and 7. This means that dendrite growth rate, G, is a constant

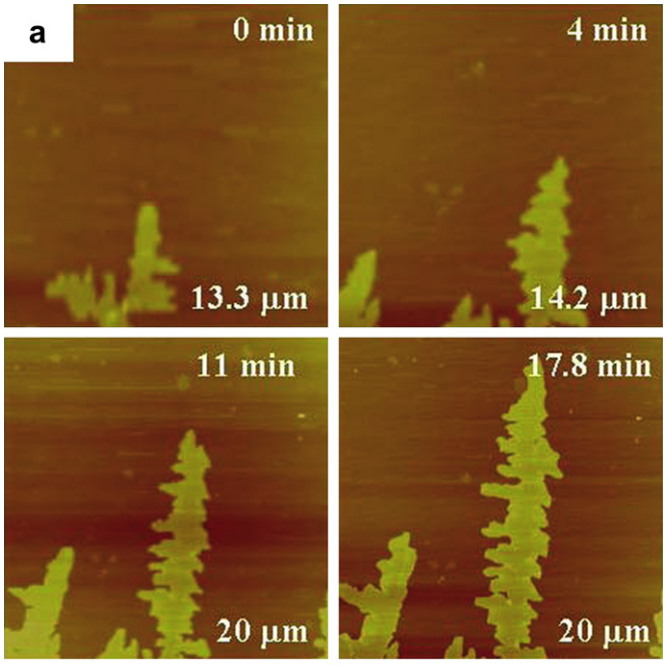

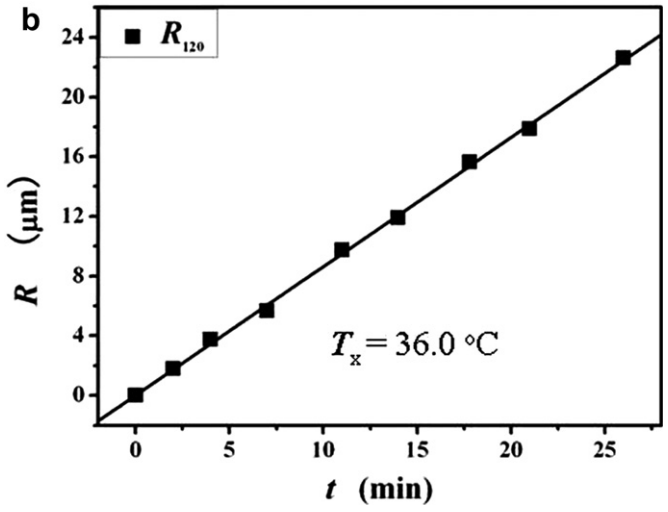

Fig. 6. (a) AFM height images present crystal growth as a function of t at T_x = 36.0 °C. (b) Plot of R versus t. R_{120} represents the length of the B-branch along <120>.

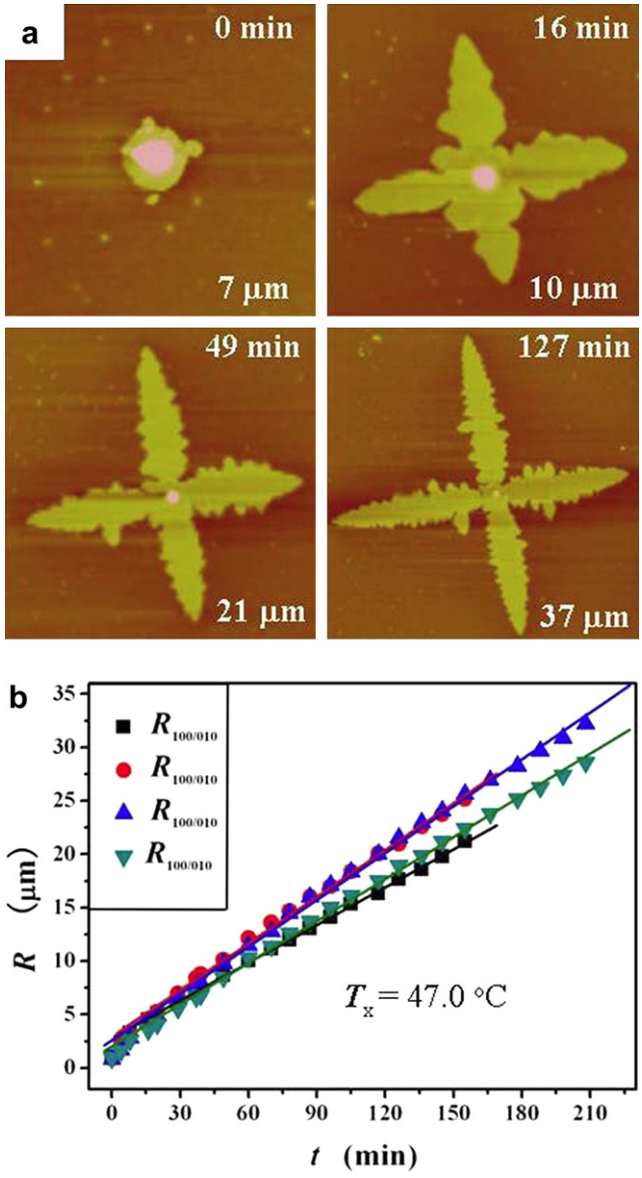

Fig. 7. (a) AFM height images present crystal growth as a function of t at T_x = 47.0 °C. (b) Plots of R versus t. $R_{100/010}$ represents the length of the NB-branch along a^* and b axes.

with respect to t. Fig. 8 shows the growth rate obtained for both the low and high T_x dendrites. The figure illustrates the expected rapid decrease of G with increasing T_x in the low T_x range. In 43.0 °C ≤ T_x ≤ 47.0 °C region however, G remains nearly a constant before decreasing again rapidly when $T_x \geq 48.0$ °C. The overall curve of G versus T_x is strongly reminiscent of plots obtained for similar MW PEO isothermal crystallization from the bulk. In the transition region from integral fold number n to a longer stem length corresponding to n-1 folds, similar growth rate variations have indeed been observed [13,14]. However, the growth mechanism is diffusion-limited in our case versus nucleation-limited in the bulk.

For the seaweeds in the range 39.0 °C ≤ T_x ≤ 42.0 °C missing in Fig. 8, G is not constant for these entities. Fig. 9 illustrates the growth of the seaweeds and the crystal size R plotted as a function of t and $t^{1/2}$. The slope of the R versus t curve decreases with increasing t, which indicates that G continuously decreases with respect to t. On the other hand, R is linearly proportional to $t^{1/2}$.

It is known that the formations of both the dendrite and seaweed crystals are controlled by a diffusion-limited mechanism.

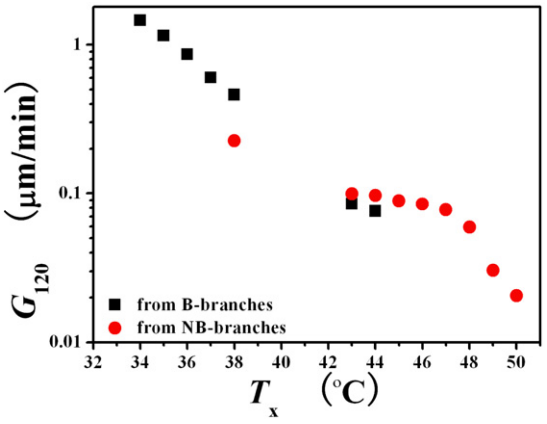

Fig. 8. Plots of G_{120} versus T_x. ■ represents the G_{120} directly measured from B-branches along <120>. ● represents the G_{120} derived from the growth rate of NB-branches along a^* and b axes, $G_{100/010}$, where $G_{120}=(\sqrt{2}/2)G_{100/010}$. In the seaweed-like crystal region of $T_x = 39.0\ ^\circ C–42.0\ ^\circ C$, the growth rate is not plotted as it is not constant versus t.

Why then should we observe a linear growth versus t in the dendrites and a linear growth versus $t^{1/2}$ in the seaweeds? Let us first point out that our observation of linear growth versus t is consistent with earlier observations on other dendrite systems [20,64–67], but no clear explanation has been proposed so far. In the following, we attempt to provide a possible explanation.

The linear growth may be explained by the following reasoning and schematic illustrations in Fig. 10. The primary branch in the dendrite is actually a quasi-1D object. Each individual growth tip is surrounded by a local supercooled PEO diffusion field. The growth of a dendrite branch generates a quasi-1D depletion zone parallel to the growth direction of the primary branch. The material transformation from supercooled melt to crystal implies $dm_c = -dm_a$, where m_c and m_a represent the masses of crystal and supercooled melt, respectively. According to Fick's first law and diffusion controlled growth in quasi-1D case,

$$\frac{\partial(\rho_c W_c H_c R)}{\partial t} = W_a \times D\frac{\partial \phi_a}{\partial x} \quad (1)$$

where ρ_c is the density of the crystal; W_c is the width of the quasi-1D crystal; H_c is the height of the crystal; R is the length of the crystal; W_a is the width of the depletion zone; φ_a represents the mass of the supercooled melt per unit area; and x is the distance from the crystal tip to a specific site ahead of the tip. Because ρ_c, W_c, H_c, and W_a are all constants at a specific T_x, we have

$$\rho_c W_c H_c \frac{\partial R}{\partial t} = DW_a \frac{\partial \phi_a}{\partial x} \quad (2)$$

then,

$$\frac{\partial R}{\partial t} = (DW_a/\rho_c W_c H_c)\frac{\partial \phi_a}{\partial x} \quad (3)$$

where $\frac{\partial \phi_a}{\partial x}$ represents the supercooled melt gradient ahead of the crystal tip. At steady state, $\frac{\partial \phi_a}{\partial x}$ is constant, and therefore, R is linearly proportional to t. This may explain why we observe the linear growth versus t even though the growth is diffusion-limited. This analysis may also provide a possible interpretation for similar observations reported in earlier works [20,64–67].

For the seaweeds, simultaneous growths of B- and NB-branches generate a 2D entity. This leads to the observation that their growths are linearly proportional to $t^{1/2}$. The mathematic analysis for this type of 2D growth was made in Ref. [29]. Therefore, the time-dependent change of growth rate from the dendrite to the seaweed is due to growth dimension change, rather than change of the growth mechanism.

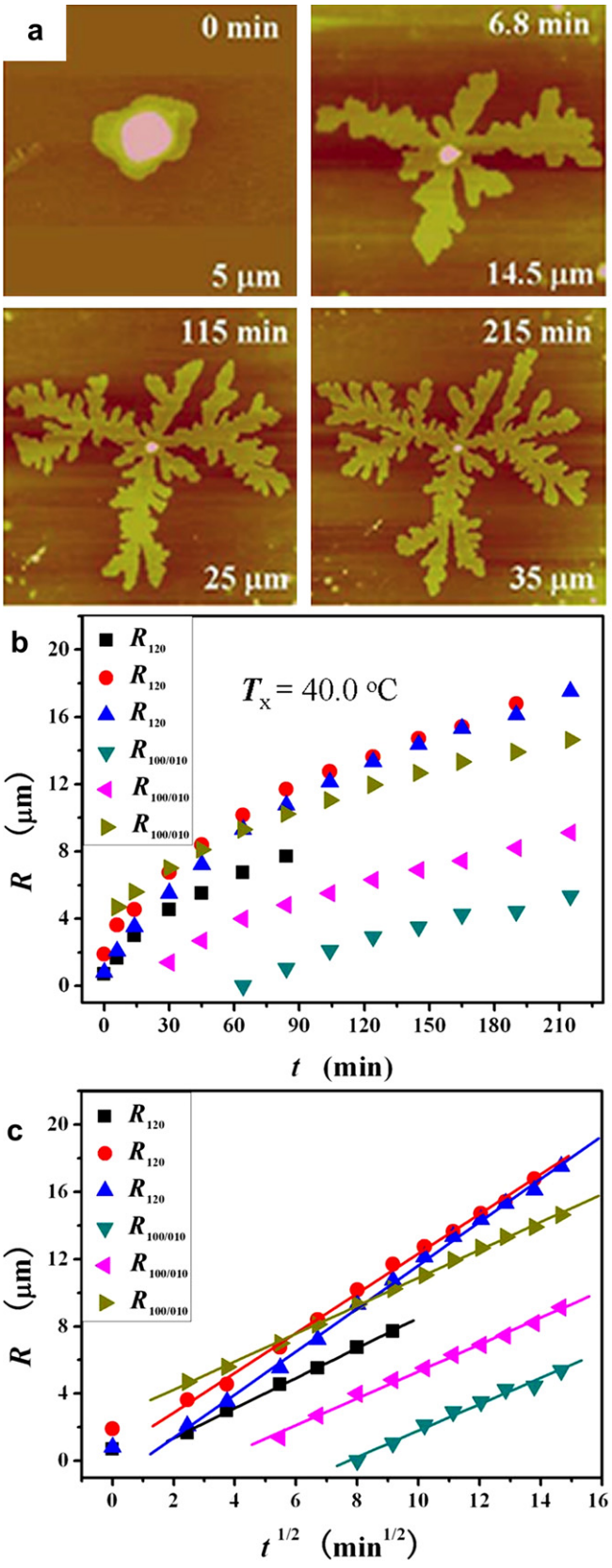

Fig. 9. (a) AFM height images present crystal growth as a function of t at $T_x = 40.0\ ^\circ C$. (b) Plots of R versus t. (c) Plots of R versus $t^{1/2}$. R_{120} represents the length of the B-branch along <120>, and $R_{100/010}$ represents the length of the NB-branch along a^* and b axes.

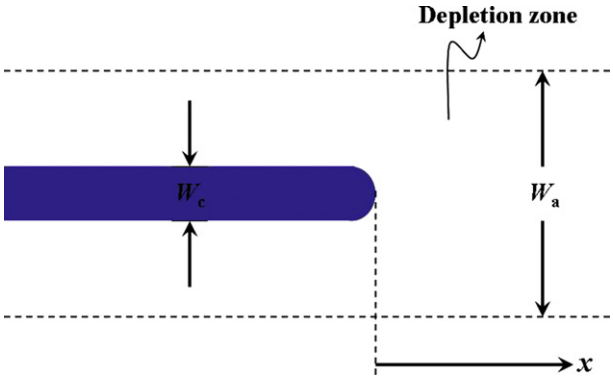

Fig. 10. Schematic illustration of 1D dendrite growth (top view).

3.4. Origin of the crystal pattern change

As illustrated in Fig. 5, the preferential crystal growth direction is along the <120> at $T_x \leq 38.0$ °C and along the a^* and b axes at $T_x \geq 43.0$ °C. Why does the fastest crystal growth direction change in these two T_x regions? Note that in the seaweed-like crystals grown at 39.0 °C $\leq T_x \leq$ 42.0 °C, three growth directions prevail. Let us analyze the growth tips of the B-branch at $T_x \leq 38.0$ °C and NB-branch at $T_x \geq 43.0$ °C. For the B-branches in $DB_{(120)}$ (Fig. 11a), the tips are flat, and correspond to the {120} planes as indicated by the SAED pattern. For the NB-branch in $DNB_{(100)/(010)}$, although the angle between two {120} planes is smaller than 90° as shown in Fig. 11b (see below for reason), the primary NB-branch grows along the merged corner of the two {120} planes. Therefore, the crystal growth planes remain the same in the entire T_x region, although the fastest growth directions are different.

In the high T_x region above 43.0 °C, the crystal growth mechanism is diffusion-limited [29]. For the diffusion coefficient, D, of PEO chains in ultrathin films, Bi et al. reported $D = 0.6 \times 10^{-14}$ m^2/s for a PEO with MW = 5.0×10^3 g/mol in the depleted zone on the surface of −OH decorated glass (that is similar to the surface of −OH decorated silicon wafer in our experiments) at 45.0 °C [68]. Based on the molecular weight dependence [69], the D value for the present PEO is 4.16 × 10^{-15} m^2/s, or 0.25 μm^2/min. The PEO growth rate, G, in the high T_x region is around 0.1–0.01 μm/min. Since G and D are comparable, a materials gradient is expected at the growth front. In turn, this speeds up the growth of the crystal tip (the a^* and b axes), although the growth planes remain the {120} planes. This leads to an angle between two {120} planes smaller than 90° (Fig. 11b). As a result, the $DNB_{(100)/(010)}$ dendrites form in this T_x region.

Next, what is the origin of the $DB_{(120)}$ dendrites formed in the region $T_x \leq 38.0$ °C? We speculate that it is because of the preferential fast growth along the <120> direction with a narrow backbone width at the {120} growth face. In this T_x region, G is much larger than D, so the crystal growth is close to the case of diffusion-limited aggregation [64]. This type of dendrite growth may rely on the fact that the primary nuclei developed in the PEO with a very small size are bounded by {120} planes. The Hoffman–Lauritzen theory predicts that when the crystal growth substrate length is smaller than a critical value that has been responsible for one nucleus and a few hundred nanometers, the growth rate along the substrate normal is faster than the growth rate after the substrate width exceeds this critical value [2,70]. One recent experimental observation has shown that the lateral spread extent increases with T_x on a length scale between 30 nm and 60 nm in single crystals of a specific polymer [71]. As shown in Fig. 2, the width of the backbone in B-branch increases with T_x, while their absolute values range from ~50 nm at $T_x = 20.0$ °C to ~320 nm at $T_x = 45.0$ °C. These width values are expected to be close to but smaller than the upper-limit of the critical substrate width at each T_x for the PEO crystal. The narrow backbone width at the growth front leads to a fast growth along the <120> directions, which results in the $DB_{(120)}$ dendrites in the region $T_x \leq 38.0$ °C.

The final question is: what are the origins of forming the B- and NB-branches? It is noted that although both growth planes are the {120} planes, the B-branches can form only when the <120> is the fastest growth direction for constructing the frames of the $DB_{(120)}$ dendrite, while the NB-branches possess a favorable growth direction along the a^* and b axes forming the $DNB_{(100)/(010)}$ dendrite. Above $T_x = 30.0$ °C, the backbones in the B-branch are more or less integrally folded-chain crystals. This indicates that the backbones are formed first with certain rearrangements resulting in integral chain crystals. Only below $T_x = 30.0$ °C can non-integral folded crystals be stabilized. It is worth mentioning that backbones in the B-branches are about 1 nm thicker than the periphery (Fig. 3). During the formation process (Fig. 6a), the thicker backbones always form ahead of the periphery, which is similar to the observation on a similar MW PEO at high T_x values [11,12]. Other parts of the crystals epitaxially grow on the backbones in the later stages with about a 1 nm thickness decrease. The thinner part may not be able to further reorganize since there is an exhausting of PEO molecules. Any thickening process would generate holes in the crystals and thus, increase the free energy and destabilize the crystals [72]. On the other hand, the NB-branches are developed from a PEO single crystal and grow along the a^* and b axes, whose tips are composed of two {120} planes. Therefore, the thickness of these two sectors of one single crystal is identical.

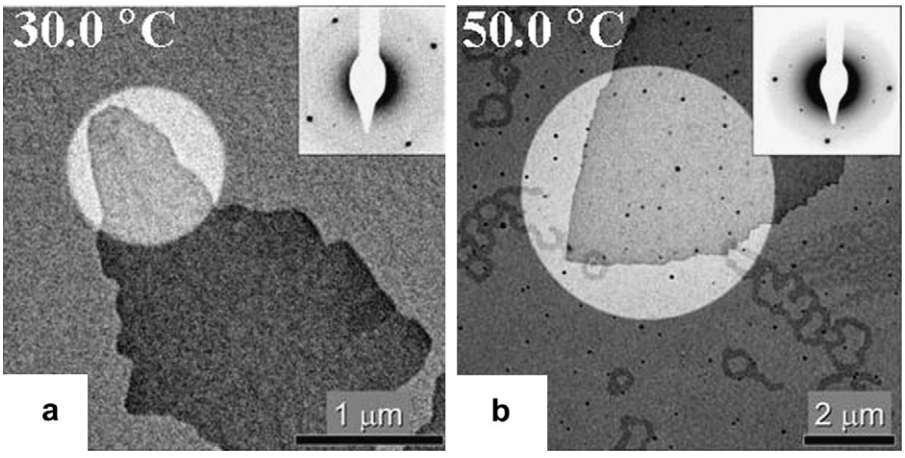

Fig. 11. (a) TEM image and SAED pattern of a B-branch tip at 30.0 °C. (b) TEM image and SAED pattern of an NB-branch tip at $T_x = 50.0$ °C.

Before concluding, it is useful to compare the present results with earlier reports on similar transitions between dendrite and seaweed type crystals. First, it must be noted that no SAED experiments were performed and therefore the crystal growth directions could not be identified [16,25,28]. As a rule, the PEO film thickness was larger or significantly larger than the crystal thickness. Also, the branching angles in seaweed crystals did not have a fixed value. Therefore, the origin of crystal growth transition was not clearly identified. In this work, the PEO film thickness is smaller than the crystal thickness. The crystal growth patterns are therefore strongly dependent on molecular diffusion. The combination of SAED analyses and crystal growth kinetics reveal that the crystal growth transitions between dendrites and seaweed result from a complex interplay of crystallographic aspects and growth mechanisms.

4. Conclusion

We have observed and analyzed T_x-dependent crystal growth patterns in a low MW PEO in ultrathin films. SAED results indicate that when $T_x \leq 38.0\,^{\circ}C$, dendritic crystals are formed with branches elongated along the <120> directions. Above $T_x = 43.0\,^{\circ}C$, dendritic crystals are also formed, but the growth directions are along the a^* or b axes. In the intermediate T_x range, $39.0\,^{\circ}C \leq T_x \leq 42.0\,^{\circ}C$, seaweed crystals are observed, in which three growth directions coexist (a^*, b and <120>). We consider that the crystal growth mechanism in the entire T_x region is a diffusion-limited process, although the crystal growth rates differ for dendrites and seaweeds because of their different growth geometries. Linear crystal growth rates are observed when $T_x \leq 38.0\,^{\circ}C$ and $T_x \geq 43.0\,^{\circ}C$ due to the 1D growth geometry of the dendrites. In the intermediate T_x region where the seaweed crystals are formed, the crystal growth is linearly proportional to $t^{1/2}$ due to the 2D growth geometry. The origin of dendrite crystals in both low and high T_x regions is also discussed. It is suggested that at $T_x \leq 38.0\,^{\circ}C$, the growth is close to diffusion-limited aggregation, and the 1D growth may be due to the fact that the substrate width of the growth front is smaller than the critical value of the nucleation event. On the other hand, in the $T_x \geq 43.0\,^{\circ}C$ region, the material gradient near the growth front generates an increase of crystal tip growth leading to the formation of dendrites with branches elongated in the a^* and b axes directions.

Acknowledgments

The Nankai group greatly appreciates the National Science Foundation of China for a grant (NSFC20474033 and 20874053) and the China Scholarship Council (CSC). Part of the work carried out at the University of Akron was supported by the National Science Foundation (DMR-0906898).

References

[1] Wunderlich B. Macromolecular physics. New York: Academic; 1973. 1976, 1980.
[2] Cheng SZD. Phase transitions in polymers: the role of metastable States. Elsevier Science; 2008.
[3] Keller A, Cheng SZD. Polymer 1998;39:4461.
[4] Cheng SZD, Keller A. Annu Rev Mater Sci 1998;28:533.
[5] Khoury F. Faraday Discuss Chem Soc 1979;68:404.
[6] Khoury F, Bolz L. Proceedings-Annual Meet Electron Microsc Soc America 1980;38:242.
[7] Khoury F, Bolz L. Bull Am Phys Soc 1985;30:493.
[8] Organ SJ, Keller A. J Mater Sci 1985;20:1571;
J Mater Sci 1985;20:1586;
J Mater Sci 1985;20:1602.
[9] Toda A. Faraday Discuss 1993;95:129.
[10] Toda A, Keller A. Colloid Polym Sci 1993;271:328.
[11] Kovacs AJ, Gonthier A, Straupe C. J Polym Sci Polym Symp 1975;50:283.
[12] Kovacs AJ, Straupe C. Faraday Discuss Chem Soc 1979;68:225.
[13] Kovacs AJ, Straupe C. J Cryst Growth 1980;48:210.
[14] Cheng SZD, Chen JH. J Polym Sci Part B Polym Phys 1991;29:311.
[15] Miller A, Mohwald H. J Chem Phys 1987;86:4258.
[16] Reiter G, Sommer JU. Phys Rev Lett 1998;80:3771;
J Chem Phys 2000;122:4376.
[17] Taguchi K, Miyaji H, Izumi K, Hoshino A, Miyamoto Y, Kokawa R. Polymer 2001;42:7443.
[18] Zhang F, Liu J, Huang H, Du B, He T. Eur Phys J E 2002;8:289.
[19] Ferreiro V, Douglas JF, Warren JA, Karim A. Phys Rev E 2002;65:042802.
[20] Ferreiro V, Douglas JF, Warren J, Karim A. Phys Rev E 2002;65:051606.
[21] Schönherr H, Frank CW. Macromolecules 2003;36:1188;
Macromolecules 2003;36:1199.
[22] Wang MT, Braun HG, Meyer E. Macromolecules 2004;37:437.
[23] Zhai XM, Wang W, Ma ZP, Wen XJ, Yuan F, Tang XF, et al. Macromolecules 2005;38:1717.
[24] Meyer E, Braun H-G. J Phys: Condensed Matter 2005;17:S623.
[25] Zhai XM, Wang W, Zhang GL, He BL. Macromolecules 2006;39:324.
[26] Flores A, Corvera-Poire E, Garza C, Castillo R. J Phys Chem B 2006;110:4824.
[27] Li BB, Esker AR. Langmuir 2007;23:2546.
[28] Okerberg BC, Marand H. J Mater Sci 2007;42:4521.
[29] Zhu DS, Liu YX, Chen EQ, Li M, Chen C, Sun YH, et al. Macromolecules 2007;40:1570.
[30] Okerberg BC, Soles CL, Douglas JF, Ro HW, Karim A. Macromolecules 2007;40:2968.
[31] Ma ZP, Zhang GL, Zhai XM, Jin LX, Tang XF, Zheng P, et al. Polymer 2008;49:1629.
[32] Zhang GL, Jin LX, Ma ZP, Zhai XM, Yang M, Zheng P, et al. J Chem Phys 2008;129:224708.
[33] Liu Y-X, Li J-F, Zhu D-S, Chen E-Q, Zhang H-D. Macromolecules 2009;42:2886.
[34] Jin LX, Zhang GL, Zhai XM, Ma ZP, Zheng P, Wang W. Polymer 2009;50:6157.
[35] Zhang GL, Jin LX, Zheng P, Shi AC, Wang W. Polymer 2010;51:554.
[36] Chen R, Li L, Zhao J. Langmuir 2010;26:5951.
[37] Chan SK, Reimer HH, Kahlweit M. J Crys Growth 1976;32:303.
[38] Langer JS. Rev Mod Phys 1980;52:1.
[39] Ben-Jacob E, Godbey R, Goldenfeld NG, Koplik J, Levine H, Mueller T, et al. Phys Rev Lett 1985;55:1315.
[40] Honjo H, Ohta S, Matsushita M. Phys Rev A 1987;36:4555.
[41] Ben-Jacob E, Garik P, Muller T, Grier D. Phys Rev A 1988;38:1370.
[42] Ben-Jacob E, Garik P. Nature (London) 1990;343:523.
[43] Ohta S, Honjo H. Phys Rev A 1991;44:8425.
[44] Brener E, Müller-Krumbhaar H, Temkin D. Europhys Lett 1992;17:535.
[45] Shochet O, Eshel BJ. Phys Rew E 1993;48:4168.
[46] Kassner K. Pattern formation in diffusion-limited crystal growth. Singapore: World Scientific; 1996.
[47] Saito Y. Statistical physics of crystal growth. Singapore: World Scientific; 1996.
[48] Meakin P. Fractals, scaling and growth far from equilibrium. Cambridge: Cambridge University Press; 1997.
[49] Bogoyavlenskiy VA, Chernova NA. Phys Rev E 2000;61:1629.
[50] Utter B, Ragnarsson R, Bodenschatz E. Phys Rev Lett 2001;86:4604.
[51] Libbrecht KG. Rep Prog Phys 2005;68:855.
[52] Haxhimali T, Karma A, Gonzales F, Rappaz M. Nat Mater 2006;5:660.
[53] Cheng SZD, Chen J, Janimak JJ. Polymer 1990;31:1018.
[54] Hobbs JK, Miles MJ. Macromolecules 2001;34:353.
[55] Organ SJ, Hobbs JK, Miles MJ. Macromolecules 2004;37:4562.
[56] Hobbs JK. Polymer 2006;47:5566.
[57] Kailas L, Vasilev C, Audinot J-N, Migeon H-N, Hobbs JK. Macromolecules 2007;40:7223.
[58] Hobbs JK, Farrance OE, Kailas L. Polymer 2009;50:4281.
[59] Cheng SZD, Chen J, Barley JS, Zhang A, Habenschuss A, Zschack PR, et al. Macromolecules 1992;25:1453.
[60] Cheng SZD, Wu SS, Chen J, Zhuo Q, Quirk RP, von Meerwall ED, et al. Macromolecules 1993;26:5101.
[61] Takahashi Y, Tadakoro H. Macromolecules 1973;6:672.
[62] Point JJ, Damman P, Janimak JJ. Polymer 1993;34:3771.
[63] Marentette JM, Brown GR. Polymer 1998;39:1405.
[64] Witten TA, Sander LM. Phys Rev Lett 1981;47:1400;
Phys Rev B 1983;27:5686.
[65] Saito Y, Ueta T. Phys Rev A 1989;40:3408.
[66] Lereah Y, Deutscher G, Grunbaum E. Phys Rev A 1991;44:8316.
[67] Couder Y, Maurer J, Gonzalez-Cinca R, Hernandez-Machado A. Phys Rev E 2005;71:031602.
[68] Bi W, Teguh JS, Yeow EKL. Phys Rev Lett 2009;102:048302.
[69] Cheng SZD, Barley JS, Von Meerwall ED. J Polym Sci Part B Polym Phys 1991;29:515.
[70] Point JJ, Colet MC, Dosière M. J Polym Sci Polym Phys Ed 1986;24:357.
[71] Alcazar D, Thierry A, Schultz P, Kawaguchi A, Cheng SZD, Lotz B. Macromolecules 2006;39:9120.
[72] Zhu DS, Liu YX, Shi AC, Chen EQ. Polymer 2006;47:5239.